Submitted to Journal of Materials Research and Technology

Direct influence of recovery behaviour on mechanical properties in oxygen-free copper processed using different SPD techniques: HPT and ECAP

Meshal Alawadhi[1,*], Shima Sabbaghianrad[2], Yi Huang[1,*], Terence. G. Langdon[1]

[1]Materials Research Group, Faculty of Engineering and the Environment, University of Southampton, Southampton SO17 1BJ, UK
[2]Department of Chemical Engineering and Materials Science, University of Southern California, Los Angeles, CA 90089-0241, USA

[*]Corresponding author: Tel: + 44-23-8059 3766
E-mail: y.huang@soton.ac.uk (Yi Huang), mya1c12@soton.ac.uk (Meshal Alawadhi)

Abstract. Oxygen-free copper of 99.95 wt.% purity was severely deformed at room temperature by two modes of severe plastic deformation, equal-channel angular pressing (ECAP) and high-pressure torsion (HPT). ECAP was performed using 4, 16 and 24 passes, and HPT was performed using 1/2, 1 and 10 turns. The results show that while recovery occurs during both ECAP and HPT processing, copper shows a faster recovery rate with HPT processing than ECAP. The occurrence of recovery was observed at an equivalent strain exceeding ~12 that led to an enhancement in the uniform plastic deformation. The influence of recovery behaviour on the mechanical properties was investigated using X-ray diffraction, microhardness and tensile testing.

Keywords: Ductility, Equal-channel angular pressing, High-pressure torsion, Recovery, Strain rate sensitivity, Work hardening.

1. Introduction

High-pressure torsion (HPT) [1–4] and equal-channel angular pressing (ECAP) [2,5–7] are the most commonly used severe plastic deformation (SPD) techniques. The HPT procedure is widely used because it has the ability to produce exceptional grain refinement [4,8] and a large fraction of high-angle grain boundaries [9] while ECAP is popular because it is a simple process that has the ability to deform larger samples which makes it a better candidate for structural applications [10–12].

It is well established that bulk ultrafine-grained (UFG) materials are successfully produced by SPD with very small grain sizes in the range between 1 μm and 100 nm [2,13–16]. UFG materials normally exhibit an extraordinary increase in strength in comparison to their coarse grain counterparts [17,18]. The inverse relationship between the yield stress (σ_y) and the square root of the grain size (d) is described by the Hall-Petch relationship [19,20]:

$$\sigma_y = \sigma_0 + k_y d^{-1/2} \quad (1)$$

where σ_0 is the lattice friction stress and k_y is a yield constant. It is readily apparent from Eq. (1) that the strength of the material increases as a consequence of the reduction in grain size. Several studies have reported the achievement of a significant grain refinement in pure Cu using ECAP [21–29] and HPT [30–41]. To date, most studies have suggested that pure Cu shows hardening behavior without recovery during both HPT [31,35,41] and ECAP [42,43] at room temperature. Nevertheless, two recent studies have reported a softening behavior of pure Cu with recovery during HPT processing [44,45]. This softening is a well-documented behavior of pure Al [46–54] and has been observed in other materials such as pure Zn [53] and pure Mg [55].

A third recent study also reported the occurrence of a recovery mechanism in pure Cu that contributed to the enhancement of ductility during 1-16 passes of ECAP at room temperature [25]. This latter report confirmed the results published in the classic study [43] that high ductility was achieved after 16 passes of ECAP as a result of grain boundary sliding. These findings were unexpected because it was previously claimed that the increase in strength in UFG materials is associated with a decrease in ductility at ambient temperature [18,56], and the poor ductility of UFG materials is due to the limited strain hardening ability [18,57,58].

Two different deformation mechanisms are proposed for the simultaneous gain in strength and ductility after processing pure Cu by ECAP for 16 passes at room temperature: one is grain boundary sliding [43] and the other is a recovery mechanism [25]. The present study is designed to clarify the mechanism leading to the enhancement in ductility by processing oxygen-free Cu for 24 passes at room temperature. Twenty-four passes was chosen instead of 16 to impose similar maximum strain on the specimen because the die angle used in this study was 110° whereas 90° was used in the previous studies. In addition, it was possible to investigate the potential for achieving high strength and ductility by imposing very high strain on the specimens using HPT since imposing a

higher strain by ECAP was limited because it was difficult to process the specimens beyond 24 passes due to the initiation of cracks.

2. Experimental materials and procedures

Oxygen-free Cu (99.95%) was used in this investigation. Billets of length 65 mm and 10 mm diameter were processed by ECAP at room temperature. These billets were pressed through a solid die having an internal channel angle, Φ, of 110º and an outer arc of curvature, Ψ, of 20º. An equivalent strain of ~0.76 was created on each separate pass based on the Φ and Ψ values [59]. The billets were pressed for 4, 16 and 24 passes repetitively and provided a maximum equivalent strain of ~18 using route B_C. In this route, the samples are rotated by 90° in the same direction between each separate pass [60]. It is well documented that route B_C is the best choice for ECAP processing to give an array of UFG microstructure with equiaxed grains separated by a high fraction of high-angle boundaries [61].

HPT processing was conducted at room temperature using disc samples with 10 mm diameter and ~0.83 mm thickness. The discs were compressed between two anvils under an applied pressure of 6.0 GPa and a torsional strain was imposed by rotating the lower anvil at a speed of 1 rpm. The discs were processed through 1/2, 1 and 10 turns using quasi-constrained conditions [62,63].

Prior to ECAP and HPT processing, the samples were annealed within a vacuum tube furnace at 600°C for 1 hour. The average grain size in the annealed sample was ~24 µm and the average Vickers microhardness was ~41 Hv.

The grain structure of oxygen-free Cu was examined by electron backscatter diffraction (EBSD) using a JEOL JSM-7001 F analytical field emission scanning electron microscope. An operating voltage of 15 kV was used during the scanning process and a step size of 0.05 µm was used to collect the EBSD patterns. The OIM images for HPT discs were taken at a distance between ~3.0 mm to ~4.0 mm from the disc centre.

The X-ray diffraction (XRD) testing was conducted on the samples after ECAP and HPT processing. A Bruker D2 Phaser X-ray diffractometer was used to analyse the whole surfaces of the samples using a copper target with Cu Kα (λ= 0.15406 nm) radiation. Recording the XRD patterns was performed by θ-2θ scans from 2θ = 40-100° and profile fitting was accomplished by Maud software. Crystallite size and microstrain were calculated based on the Rietveld method using Maud software and their values were used to calculate the dislocation density.

Vickers microhardness measurements were recorded using a Future-Tech FM-300 microhardness tester. 100 gf was used during the hardness indentations with a 15 s dwell time. For HPT, the average values were recorded along the radius (5.0 mm) of each disc with 0.3 mm between each indentation point. Four indentations were measured around each of these points, separated by a distance of 0.15 mm, then the average for these four points was calculated. For ECAP, the microhardness measurements were

recorded along the longitudinal axis of the ECAP billets over a distance of 25 mm with 0.5 mm separation between each indentation point.

For tensile testing, tensile specimens were machined from HPT discs and ECAP billets using electrical discharge machining. The HPT specimen had a gauge length of 1.0 mm and cross-sectional area of 1.0 x 0.8 mm^2 as shown in Fig. 1(a) and the ECAP specimen had a gauge length of 4.0 mm and cross-sectional area of 3.0 x 2.0 mm^2 as shown in Fig. 1(b). A Zwick Z030 testing machine was used for pulling the specimens at room temperature using initial strain rates of $1.0x10^{-4}$ s^{-1} and $1.0x10^{-3}$ s^{-1}.

3. Experimental Results

3.1 Microstructure after deformation

Fig. 2 presents OIM images for oxygen-free copper after processing by ECAP for 4 and 24 passes and HPT for 1/2 and 10 turns. The difference in colors represents the difference in the grain misorientations as denoted by the unit triangle.

After 4 passes of ECAP, the grains were mostly large and elongated with a scattering of small grains as shown in Fig. 2(a). The average grain size was ~4.5 μm and the fraction of high-angle grain boundaries (HAGBs) was ~65%. HAGBs are defined as boundaries with misorientations larger than 15°, whereas boundaries with misorientations between 2° and 15° are defined as low-angle grain boundaries (LAGBs). A significant grain refinement was observed after 24 passes as displayed in Fig. 2(b). The microstructure evolved into reasonable homogeneity with ultrafine and equiaxed grains having an average grain size of ~600 nm and ~90% of HAGBs.

After 1/2 turn of HPT shown in Fig. 2(c), a rapid evolution towards microstructural homogeneity was observed. The microstructure consisted of ultrafine and equiaxed grains with an average size of ~700 nm and ~85% of HAGBs. A further grain refinement was observed after deforming the disc with 10 turns as displayed in Fig. 2(d). High strain deformation produced an average grain size of ~500 nm with ~82% of HAGBs.

3.2 XRD analysis

The values of the calculated dislocation densities and crystallite sizes obtained from XRD measurements are shown in Fig. 3. The dislocation density was calculated based on the data obtained from XRD analysis using the equation [64,65]:

$$\rho = \frac{2\sqrt{3}<\varepsilon^2>^{1/2}}{D_C b} \quad (2)$$

where $< \varepsilon^2 >^{1/2}$ is the lattice microstrain, D_C is the average crystallite size and b is the Burgers vector. The XRD analysis on the annealed condition showed a dislocation density of ~3.9 x 10^{12} m^{-2} and a crystallite size of ~480 nm.

During ECAP processing, the dislocation density increased to ~8.2 x 10^{13} m^{-2} after 4 passes and then increased further to ~4.0 x 10^{14} m^{-2} after 16 passes, followed by a decrease to a value of ~2.2 x 10^{14} m^{-2} after 24 passes, as shown in Fig. 3(a). The crystallite size, on the other hand, decreased from ~480 nm to ~172 nm after 4 passes and ~111 nm after 16 passes then increased to ~134 nm after 24 passes as in Fig. 3(a).

During HPT processing, the dislocation density increased to ~5.6 x 10^{13} m^{-2} after 1/2 turn followed by a decrease to values of ~3.2 x 10^{13} m^{-2} and ~2.8 x 10^{13} m^{-2} after 1 and 10 turns, respectively, as shown in Fig. 3(b). The crystallite size decreased to ~132 nm after 1/2 turn then increased to ~154 nm and ~179 after 1 and 10 turns, respectively.

3.3 Microhardness measurements

For the ECAP specimens, the microhardness measurements were recorded along the longitudinal axes of the billets. It is readily apparent from Fig. 4(a) that the average hardness increased significantly to ~110 Hv after 4 ECAP passes in comparison to ~41 Hv measured for the annealed condition. The average hardness further increased to ~120 Hv after 16 passes. This was followed by a drop after 24 passes to ~112 Hv.

The microhardness measurements were recorded along the 5 mm radius of the discs processed by HPT as shown in Fig. 4(b). The variation of microhardness measurements between the centre and edge positions in the HPT discs was neglected in this study. It follows from Fig. 4(b) that a substantial increase in the average hardness was recorded after 1/2 turn during HPT processing. The average hardness increased to ~133 Hv after 1/2 turn then saturated at a lower value of ~127 Hv after 10 turns.

3.4 Tensile properties

Fig. 5 shows engineering stress-engineering strain curves truncated to the peak stress, which demonstrate the strain hardening behavior for a) ECAP and b) HPT samples when tested at 1.0 x 10^{-4} s^{-1}. The values of the tensile properties are summarized in Table 1. As can be seen from Fig. 5(a), the mechanical strength increased for up to 16 passes followed by a drop after 24 passes. This drop in strength was associated with an increase in the uniform elongation from 2.1% to 3.6%. The same trend was observed during HPT, however it occurred at a faster rate. The mechanical strength decreased after 1 turn while the uniform elongation increased with further strain, as in Fig. 5(b).

4. Discussion

Earlier research demonstrated that grain boundary sliding is the reason for the enhancement of both strength and ductility due to the increase of strain rate sensitivity [43]. The paradox of strength and ductility was first observed by processing pure Cu by ECAP for up to 16 passes and pure Ti by HPT for 5 turns at room temperature. However, this study has not focused on the intrinsic properties of the material. In the present study, oxygen-free Cu was processed by ECAP and HPT and then the crystallite size and

dislocation density were examined and correlated with the mechanical properties such as microhardness and tensile properties. It was found that the hardness and strength dropped slightly at a certain strain while uniform plastic elongation of the specimens was enhanced by processing using either ECAP or HPT.

UFG materials normally show an onset of early necking when pulled in tension, due to their low work hardening rate and low strain rate sensitivity after SPD processing which leads to a fall in their uniform plastic deformation. The high rate of work hardening is caused by the accumulation of dislocations within the grains; however in UFG metals the grains are small which makes dislocation storage more difficult [58]. Dislocations are emitted and absorbed at the grain boundaries instead of accumulating within the grain interior. Thus, most UFG metals exhibit limited ductility at room temperature [66]. The low hardening capacity in nanostructured Cu produced by ECAP was discussed in an earlier study and three strategies were suggested to prolong the uniform tensile deformation [67]. These strategies included creating a microstructure with a bimodal grain size distribution, deforming the material at a low temperature and/or high strain rates and increasing the strain rate sensitivity [67].

The strain rate sensitivity is a crucial factor that is considered when evaluating the strain hardening of the material. According to Hart's criterion, increasing the strain rate sensitivity can delay the onset of localized deformation and prolong the ductility of the material [68]. UFG materials tend to exhibit higher strain rate sensitivity at low temperatures in comparison to their coarse-grained counterparts [69,70]. The strain rate sensitivity for polycrystalline materials is defined as [68]:

$$m = \left(\frac{\partial ln\sigma}{\partial ln\dot{\varepsilon}}\right)_{\varepsilon} \quad (3)$$

where σ is the true stress and $\dot{\varepsilon}$ the strain rate. In practice, it is well documented that a large value of m in the presence of small grains and a large fraction of HAGBs can trigger grain boundary sliding [71]. It has been reported that grain boundary sliding occurred in UFG Cu during the ECAP process at room temperature [12,43]. The occurrence of grain boundary sliding generally requires a high homologous temperature (~$0.5T_m$) [72,73], however, it has been reported that grain boundary sliding also occurs at lower temperatures during ECAP and HPT processing [12,74–76]. The grain boundaries are in a nonequilibrium state during processing by ECAP or HPT due to the surplus of extrinsic dislocations which are not geometrically necessary [7] and grain boundary sliding is therefore facilitated by their movement [77].

Thus, in order to investigate the influence of the strain rate sensitivity on the ductility of the Cu specimens, another set of samples were pulled in tension using a uniaxial tensile test at a strain rate of $1.0x10^{-3}$ s^{-1} in order to calculate the strain rate sensitivity using equation (3). Initially, the m value of the annealed specimen was ~0.0083. The strain rate sensitivity increases with increasing number of ECAP passes as well as increasing HPT turns. The calculated m values of the ECAP specimens were ~0.00941, ~0.0193 and ~0.0216 for 4, 16 and 24 passes, respectively, whereas for the

HPT specimens were ~0.036, ~0.039 and ~0.045 for 1/2, 1 and 10 turns, respectively. This is in agreement with an earlier report showing an increase in the strain rate sensitivity from 0.007 to 0.023 after processing pure Cu by ECAP from 1 to 12 passes [78]. There may be a small contribution towards the delay of the onset of early necking by increasing the strain rate sensitivity with ECAP passes and HPT turns, however the value is very small to facilitate grain boundary sliding.

The work hardening rate of the material is another factor contributing to the onset of the localized deformation during tensile testing as given by the Considère criterion [79,80]:

$$\left(\frac{\partial\sigma}{\partial\varepsilon}\right)_{\dot{\varepsilon}} \leq \sigma, \tag{4}$$

where σ is the true stress, ε is the true strain and $\dot{\varepsilon}$ is the strain rate. Plastic instability occurs when the work hardening rate $\left(\frac{\partial\sigma}{\partial\varepsilon}\right)$ becomes equal to or less than the flow stress during tension. Generally, the grains become smaller with increasing strain during SPD processing which decreases the dislocation storage capacity and limits the uniform deformation. Fig. 6 presents the work hardening rate as a function of the true stress for oxygen-free Cu processed by a) ECAP and b) HPT. It is readily apparent from Fig. 6(a) that the specimen processed by ECAP for 24 passes exhibited a higher work hardening rate than the specimen processed by 4 passes. Also, it is apparent from Fig. 6(b) that the specimen processed by HPT for 10 turns exhibited a higher work hardening rate than the specimen processed by 1/2 turn. This indicates that the work hardening rate increases with numbers of passes or turns.

As shown in Fig. 3(a) the crystallite size decreases with increasing numbers of passes and reaches a minimum value in the region of 16 passes but then increases at 24 passes. On the other hand, there is a maximum in the dislocation density for a specimen processed by 16 passes, after which the density decreases. Similar trends were observed in Fig. 3(b) during the HPT process, where the crystallite size reached a minimum after 1/2 turn then increased with further straining, whereas the maximum value of the dislocation density occurred with the specimen subjected to 1/2 turn after which a rapid drop was observed at 1 turn followed by a continuous and gradual decrease in the dislocation density up to 10 turns. These trends of crystallite size and dislocation density displayed in Fig. 3(a) for ECAP specimens and in Fig. 3(b) for HPT specimens matches the drop in microhardness values shown in Fig. 4(a-b) and are also in a good agreement with the decrease in the strength shown in Fig. 5(a-b). These observations suggests the occurrence of a recovery mechanism during ECAP and HPT processing.

In the present study, the occurrence of the recovery mechanism highly influences the work hardening rate of oxygen-free Cu. The increase of the uniform plastic deformation presented in Table 1 is due to the decrease in both strength and dislocation densities observed during both processes, as shown in Fig. 3(a) and Fig. 3(b). This decrease in the dislocation density enhances the dislocation storage and increases the ability to accommodate more dislocations and regain the capacity of work hardening. The

decrease in the dislocation density with the increase in the crystallite size is attributed to the recovery mechanism occurring during the ECAP and HPT processing that increases the mean free path of dislocations thus increasing the work hardening rate. This is consistent with a previous study on pure Cu processed by ECAP for 16 passes at room temperature [25].

A close inspection of Fig. 3 shows that the occurrence of the recovery mechanism during HPT is faster than for ECAP. This may be due to the intensive strain imposed by HPT. Accordingly, the equivalent strains for ECAP specimens are calculated using [59]:

$$\varepsilon_N = \frac{N}{\sqrt{3}}\left[2\cot\left(\frac{\Phi}{2}+\frac{\Psi}{2}\right)+\Psi\mathrm{cosec}\left(\frac{\Phi}{2}+\frac{\Psi}{2}\right)\right] \quad (5)$$

where N is the number of passes, Φ is the internal channel angle and Ψ is the outer arc of curvature. The equivalent strains for 4, 16 and 24 passes are ~3, ~12 and ~18, respectively.

The equivalent strains for HPT specimens were calculated using [81]:

$$\varepsilon = \frac{2\pi r N}{h\sqrt{3}} \quad (6)$$

where N is the number of rotations, r is the distance from the disc centre and h is the thickness of the disc. Since the strain varies across the disc, an average strain is calculated for each condition. The equivalent strains for 1/2, 1 and 10 turns are ~7, ~16 and ~173, respectively. It is readily apparent that the recovery mechanism takes place at an equivalent strain exceeding ~12. Thus, it is concluded that uniform plastic deformation can be prolonged by deforming the oxygen-free Cu beyond a certain equivalent strain.

5. Summary and conclusions

1. Dislocation density and crystallite size for oxygen-free Cu both decreased after deformation by ECAP and HPT, however, at a certain strain the dislocation density decreased while the crystallite size increased indicating the occurrence of a recovery mechanism. The occurrence of this recovery is much faster during HPT than ECAP. This is attributed to the intensive strain imposed by HPT.
2. Microhardness measurements are in agreement with the XRD results. The Hv values decreased after 24 ECAP passes and after 1 turn of HPT. The microhardness values increased significantly after ECAP and HPT deformation by comparison to the annealed condition.
3. Although the strain rate sensitivity values are very small, it appears that it assists in the delay of early necking but not to the extent of facilitating a grain boundary sliding mechanism.
4. The uniform plastic elongation of oxygen-free Cu was enhanced after ECAP and HPT processing as a result of the recovery mechanism whereby the dislocation annihilation process reduces the dislocation density in the presence of high-angle

grain boundaries and also due to the increase in the crystallite size, which increases the mean free path of dislocations and restores the work-hardening ability of the material.

5. The uniform plastic elongation is improved in oxygen-free Cu by imposing equivalent strains higher than ~12.

Acknowledgements

This research was presented at the 3rd Pan American Materials Congress held as part of the TMS Annual Meeting in San Diego, California, on February 27 - March 2, 2017. This work was supported by the European Research Council under ERC Grant Agreement No. 267464-SPDMETALS and by the Public Authority for Applied Education and Training (PAAET) in Kuwait.

References

[1] Zhilyaev AP, Langdon TG. Using high-pressure torsion for metal processing: Fundamentals and applications. Prog Mater Sci 2008;53:893–979.

[2] Valiev RZ, Islamgaliev RK, Alexandrov I V. Bulk nanostructured materials from severe plastic deformation. Prog Mater Sci 2000;45:103–89.

[3] Smirnova N, Levit V, Pilyugin V, Kuznetsov R, Davydova L, Sazonova V. FCC structure evolution for single crystals under large plastic strains. Fiz Met Met 1986;61:1170.

[4] Zhilyaev AP, Nurislamova G V., Kim B-K, Baró MD, Szpunar JA, Langdon TG. Experimental parameters influencing grain refinement and microstructural evolution during high-pressure torsion. Acta Mater 2003;51:753–65.

[5] Valiev RZ, Langdon TG. Principles of equal-channel angular pressing as a processing tool for grain refinement. Prog Mater Sci 2006;51:881–981.

[6] Segal VM, Reznikov VI, Drobyshevskiy AE, Kopylov VI. Plastic working of metals by simple shear. Russ Met 1981;1:99–105.

[7] Valiev RZ, Korznikov A V., Mulyukov RR. Structure and properties of ultrafine-grained materials produced by severe plastic deformation. Mater Sci Eng A 1993;168:141–8.

[8] Zhilyaev AP, Lee S, Nurislamova G V., Valiev RZ, Langdon TG. Microhardness and microstructural evolution in pure nickel during high-pressure torsion. Scr Mater 2001;44:2753–8.

[9] Wongsa-Ngam J, Kawasaki M, Langdon TG. A comparison of microstructures and mechanical properties in a Cu-Zr alloy processed using different SPD techniques.

J Mater Sci 2013;48:4653–60.

[10] Valiev RZ, Krasilnikov N, Tsenev NK. Plastic deformation of alloys with submicron-grained structure. Mater Sci Eng A 1991;137:35–40.

[11] Wang J, Furukawa M, Horita Z, Nemoto M, Valiev RZ, Langdon TG. Enhanced grain growth in an AI-Mg alloy with ultrafine grain size. Mater Sci Eng A 1996;216:41–6.

[12] Valiev RZ, Kozlov E V., Ivanov YF, Lian J, Nazarov AA, Baudelet B. Deformation behaviour of ultra-fine-grained copper. Acta Metall Mater 1994;42:2467–75.

[13] Segal VM. Materials processing by simple shear. Mater Sci Eng A 1995;197:157–64.

[14] Valiev RZ. Structure and mechanical properties of ultrafine-grained metals. Mater Sci Eng A 1997;234–236:59–66.

[15] Iwahashi Y, Horita Z, Nemoto M, Langdon TG. The process of grain refinement in equal-channel angular pressing. Acta Mater 1998;46:3317–31.

[16] Horita Z, Fujinami T, Nemoto M, Langdon TG. Equal-channel angular pressing of commercial aluminum alloys: Grain refinement, thermal stability and tensile properties. Metall Mater Trans A 2000;31:691–701.

[17] Valiev RZ. Nanomaterial advantage. Nature 2002;419:887–9.

[18] Zhu YT, Liao X. Nanostructured metals: retaining ductility. Nat Mater 2004;3:351–2.

[19] Hall EO. The Deformation and Ageing of Mild Steel: III Discussion of Results. Proc Phys Soc B 1951;64:747–53.

[20] Petch NJ. The Cleavage Strength of Polycrystals. J Iron Steel Inst 1953;174:25–8.

[21] Komura S, Horita Z, Nemoto M, Langdon TG. Influence of stacking fault energy on microstructural development in equal-channel angular pressing. J Mater Res 1999;14:4044–50.

[22] Huang WH, Chang L, Kao PW, Chang CP. Effect of die angle on the deformation texture of copper processed by equal channel angular extrusion. Mater Sci Eng A 2001;307:113–8.

[23] Hoppel HW, Zhou ZM, Mughrabi H, Valiev RZ. Microstructural study of the parameters governing coarsening and cyclic softening in fatigued ultrafine-grained copper. Philos Mag A 2002;82:1781–94.

[24] Wu SD, Wang ZG, Jiang CB, Li GY, Alexandrov IV, Valiev RZ. The formation of PSB-like shear bands in cyclically deformed ultrafine grained copper processed by ECAP. Scr Mater 2003;48:1605–9.

[25] Dalla Torre F, Lapovok R, Sandlin J, Thomson PF, Davies CHJ, Pereloma EV. Microstructures and properties of copper processed by equal channel angular

extrusion for 1–16 passes. Acta Mater 2004;52:4819–32.

[26] Jiang QW, Li XW. Effect of pre-annealing treatment on the compressive deformation and damage behavior of ultrafine-grained copper. Mater Sci Eng A 2012;546:59–67.

[27] Stepanov ND, Kuznetsov A V., Salishchev GA, Raab GI, Valiev RZ. Effect of cold rolling on microstructure and mechanical properties of copper subjected to ECAP with various numbers of passes. Mater Sci Eng A 2012;554:105–15.

[28] Huang CX, Hu W, Yang G, Zhang ZF, Wu SD, Wang QY, et al. The effect of stacking fault energy on equilibrium grain size and tensile properties of nanostructured copper and copper-aluminum alloys processed by equal channel angular pressing. Mater Sci Eng A 2012;556:638–47.

[29] Zhilyaev AP, Langdon TG. Microhardness and EBSD microstructure mapping in partially-pressed Al and Cu through 90º ECAP die. Mater Res 2013;16:586–91.

[30] Lugo N, Llorca N, Cabrera JM, Horita Z. Microstructures and mechanical properties of pure copper deformed severely by equal-channel angular pressing and high pressure torsion. Mater Sci Eng A 2008;477:366–71.

[31] Jiang H, Zhu YT, Butt DP, Alexandrov I V, Lowe TC. Microstructural evolution, microhardness and thermal stability of HPT-processed Cu. Mater Sci Eng A 2000;290:128–38.

[32] Hebesberger T, Stüwe HP, Vorhauer A, Wetscher F, Pippan R. Structure of Cu deformed by high pressure torsion. Acta Mater 2005;53:393–402.

[33] Horita Z, Langdon TG. Microstructures and microhardness of an aluminum alloy and pure copper after processing by high-pressure torsion. Mater Sci Eng A 2005;410–411:422–5.

[34] Ungár T, Balogh L, Zhu YT, Horita Z, Xu C, Langdon TG. Using X-ray microdiffraction to determine grain sizes at selected positions in disks processed by high-pressure torsion. Mater Sci Eng A 2007;444:153–6.

[35] Edalati K, Fujioka T, Horita Z. Microstructure and mechanical properties of pure Cu processed by high-pressure torsion. Mater Sci Eng A 2008;497:168–73.

[36] Kilmametov AR, Vaughan G, Yavari AR, LeMoulec A, Botta WJ, Valiev RZ. Microstructure evolution in copper under severe plastic deformation detected by in situ X-ray diffraction using monochromatic synchrotron light. Mater Sci Eng A 2009;503:10–3.

[37] An XH, Wu SD, Zhang ZF, Figueiredo RB, Gao N, Langdon TG. Evolution of microstructural homogeneity in copper processed by high-pressure torsion. Scr Mater 2010;63:560–3.

[38] Edalati K, Miresmaeili R, Horita Z, Kanayama H, Pippan R. Significance of temperature increase in processing by high-pressure torsion. Mater Sci Eng A 2011;528:7301–5.

[39] Al-Fadhalah KJ, Alhajeri SN, Almazrouee AI, Langdon TG. Microstructure and microtexture in pure copper processed by high-pressure torsion. J Mater Sci 2013;48:4563–72.

[40] Almazrouee AI, Al-Fadhalah KJ, Alhajeri SN, Langdon TG. Microstructure and microhardness of OFHC copper processed by high-pressure torsion. Mater Sci Eng A 2015;641:21–8.

[41] Edalati K, Ito Y, Suehiro K, Horita Z. Softening of high purity aluminum and copper processed by high pressure torsion. Int J Mater Res 2009;100:1668–73.

[42] Lugo N, Llorca N, Suñol JJ, Cabrera JM. Thermal stability of ultrafine grains size of pure copper obtained by equal-channel angular pressing. J Mater Sci 2010;45:2264–73.

[43] Valiev RZ, Alexandrov I V. Paradox of strength and ductility in metals processed by severe plastic deformation. Mater Res Soc 2002:5–8.

[44] Huang Y, Sabbaghianrad S, Almazrouee AI, Al-Fadhalah KJ, Alhajeri SN, Langdon TG. The significance of self-annealing at room temperature in high purity copper processed by high-pressure torsion. Mater Sci Eng A 2016;656:55–66.

[45] Xu J, Li J, Wang CT, Shan D, Guo B, Langdon TG. Evidence for an early softening behavior in pure copper processed by high-pressure torsion. J Mater Sci 2016;51:1923–30.

[46] Xu C, Horita Z, Langdon T. The evolution of homogeneity in processing by high-pressure torsion. Acta Mater 2007;55:203–12.

[47] Harai Y, Ito Y, Horita Z. High-pressure torsion using ring specimens. Scr Mater 2008;58:469–72.

[48] Ito Y, Horita Z. Microstructural evolution in pure aluminum processed by high-pressure torsion. Mater Sci Eng A 2009;503:32–6.

[49] Edalati K, Horita Z. Scaling-up of high pressure torsion using ring shape. Mater Trans 2009;50:92–5.

[50] Kawasaki M, Ahn B, Langdon TG. Effect of strain reversals on the processing of high-purity aluminum by high-pressure torsion. J Mater Sci 2010;45:4583–93.

[51] Xu C, Horita Z, Langdon TG. Microstructural evolution in pure aluminum in the early stages of processing by high-pressure torsion. Mater Trans 2010;51:2–7.

[52] Kawasaki M, Figueiredo RB, Langdon TG. An investigation of hardness homogeneity throughout disks processed by high-pressure torsion. Acta Mater 2011;59:308–16.

[53] Edalati K, Horita Z. Significance of homologous temperature in softening behavior and grain size of pure metals processed by high-pressure torsion. Mater Sci Eng A 2011;528:7514–23.

[54] Edalati K, Horita Z, Furuta T, Kuramoto S. Dynamic recrystallization and recovery

during high-pressure torsion: Experimental evidence by torque measurement using ring specimens. Mater Sci Eng A 2013;559:506–9.

[55] Edalati K, Yamamoto A, Horita Z, Ishihara T. High-pressure torsion of pure magnesium: Evolution of mechanical properties, microstructures and hydrogen storage capacity with equivalent strain. Scr Mater 2011;64:880–3.

[56] Koch C. Optimization of strength and ductility in nanocrystalline and ultrafine grained metals. Scr Mater 2003;49:657–62.

[57] Van Swygenhoven H, Weertman JR. Preface to the viewpoint set on: mechanical properties of fully dense nanocrystalline metals. Scr Mater 2003;49:625–7.

[58] Budrovic Z, Van Swygenhoven H, Derlet PM, Van Petegem S, Schmitt B. Plastic Deformation with Reversible Peak Broadening in Nanocrystalline Nickel. Science 2004;304:273–7.

[59] Iwahashi Y, Wang J, Horita Z, Nemoto M, Langdon TG. Principle of equal-channel angular pressing for the processing of ultrafine-grained materials. Scr Mater 1996;35:143–6.

[60] Furukawa M, Iwahashi Y, Horita Z, Nemoto M, Langdon TG. The shearing characteristics associated with equal-channel angular pressing. Mater Sci Eng A 1998;257:328–32.

[61] Oh-ishi K, Horita Z, Furukawa M, Nemoto M, Langdon TG. Optimizing the Rotation Conditions for Grain Refinement in Equal-Channel Angular Pressing. Metall Mater Trans A 1998;29A:2011–3.

[62] Figueiredo RB, Cetlin PR, Langdon TG. Using finite element modeling to examine the flow processes in quasi-constrained high-pressure torsion. Mater Sci Eng 2011;A528:8198–204.

[63] Figueiredo RB, Pereira PHR, Aguilar MTP, Cetlin PR, Langdon TG. Using finite element modeling to examine the temperature distribution in quasi-constrained high-pressure torsion. Acta Mater 2012;60:3190–8.

[64] Williamson G, Smallman R. III. Dislocation densities in some annealed and cold-worked metals from measurements on the X-ray debye-scherrer spectrum. Philos Mag 1956;1:34–46.

[65] Smallman R, Westmacott K. Stacking faults in face-centred cubic metals and alloys. Philos Mag 1957;2:669–83.

[66] Jia D, Wang YM, Ramesh KT, Ma E, Zhu YT, Valiev RZ. Deformation behavior and plastic instabilities of ultrafine-grained titanium. Appl Phys Lett 2001;79:611.

[67] Wang YM, Ma E. Three strategies to achieve uniform tensile deformation in a nanostructured metal. Acta Mater 2004;52:1699–709.

[68] Meyers MA, Chawla KK. Mechanical metallurgy, Englewood Cliffs (NJ): Prentice-Hall; 1984, pp. 570–85.

[69] Zhao Y, Zhu YT, Lavernia EJ. Strategies for improving tensile ductility of bulk nanostructured materials. Adv Eng Mater 2010;12:769–78.

[70] Ma E. Eight routes to improve the tensile ductility of bulk nanostructured metals and alloys. Jom 2006;58(4):49–53.

[71] Zhao YH, Bingert JF, Zhu YT, Liao XZ, Valiev RZ, Horita Z, et al. Tougher ultrafine grain Cu via high-angle grain boundaries and low dislocation density. Appl Phys Lett 2008;92:10–3.

[72] Gifkins RC, Langdon TG. On the question of low- temperature sliding at grain boundaries. J Inst Met 1965;93:347.

[73] Langdon TG. Grain boundary sliding revisited : Developments in sliding over four decades 2006;1:597–609.

[74] Chinh NQ, Szommer P, Horita Z, Langdon TG. Experimental evidence for grain-boundary sliding in ultrafine-grained aluminum processed by severe plastic deformation. Adv Mater 2006;18:34–9.

[75] Valiev RZ, Yu M. Unusual super-ductility at room temperature in an ultrafine-grained aluminum alloy 2010:4718–24.

[76] Polyakov A V., Semenova IP, Valiev RZ, Huang Y, Langdon TG. Influence of annealing on ductility of ultrafine-grained titanium processed by equal-channel angular pressing–Conform and drawing. MRS Commun 2013;3:249–53.

[77] Valiev R. Nanostructuring of metals by severe plastic deformation for advanced properties. Nat Mater 2004;3:511–6.

[78] Dalla Torre FH, Pereloma E V., Davies CHJ. Strain hardening behaviour and deformation kinetics of Cu deformed by equal channel angular extrusion from 1 to 16 passes. Acta Mater 2006;54:1135–46.

[79] Dieter GE. Mechanical Metallurgy. Singapore: McGraw-Hill; 1988.

[80] Hart EW. Theory of the tensile test. Acta Metall 1967;15:351–5.

[81] Valiev RZ, Ivanisenko Y V., Rauch EF, Baudelet B. Structure and deformation behaviour of armco iron subjected to severe plastic deformation. Acta Mater 1996;44:4705–12.

Figure captions

Fig. 1 Schematic illustration showing the dimensions of the miniature tensile specimens cut from a) ECAP billet and b) HPT disc.

Fig. 2 EBSD orientation images showing the evolution of microstructure in oxygen-free copper specimens after ECAP processing through a) 4 passes, b) 24 passes and after HPT processing through c) 1/2 turn, d) 10 turns.

Fig. 3 Dislocation density and crystallite size as a function of the number of a) ECAP passes and b) HPT turns.

Fig. 4 Vickers microhardness measurements for oxygen-free Cu a) along the longitudinal axis of the ECAP billet and b) along the radius of the HPT discs.

Fig. 5 Truncated engineering stress – engineering strain curves demonstrating the strain hardening behaviour for a) ECAP and b) HPT specimens.

Fig. 6 Work hardening rate as a function of true stress for oxygen-free Cu deformed by a) ECAP and b) HPT.

Table captions

Table 1. Values of yield stress (YS), ultimate tensile stress (UTS) and uniform elongation (UEL%) for Cu specimens subjected to HPT and ECAP.

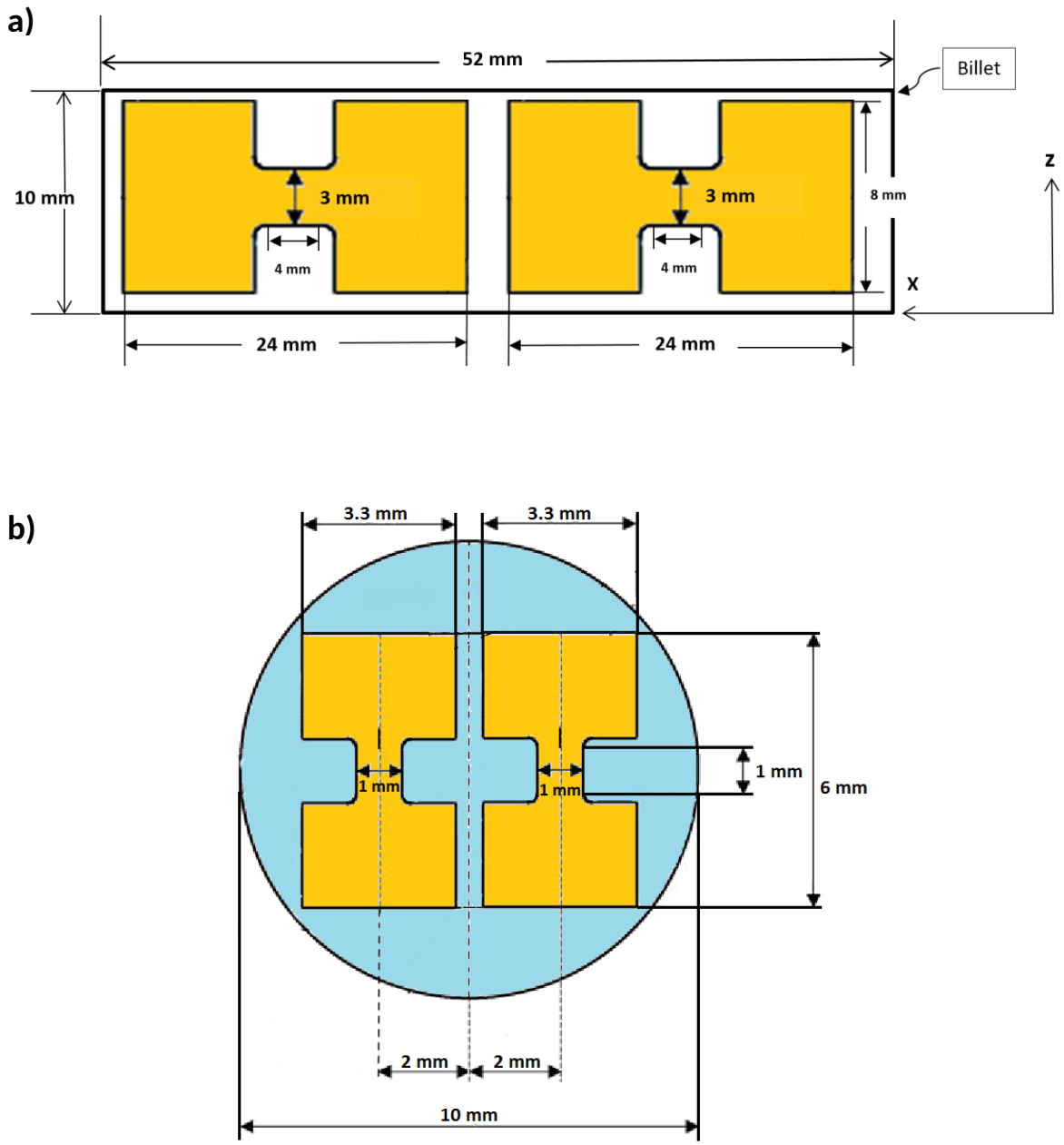

Fig. 1 Schematic illustration showing the dimensions of the miniature tensile specimens cut from a) ECAP billet and b) HPT disc.

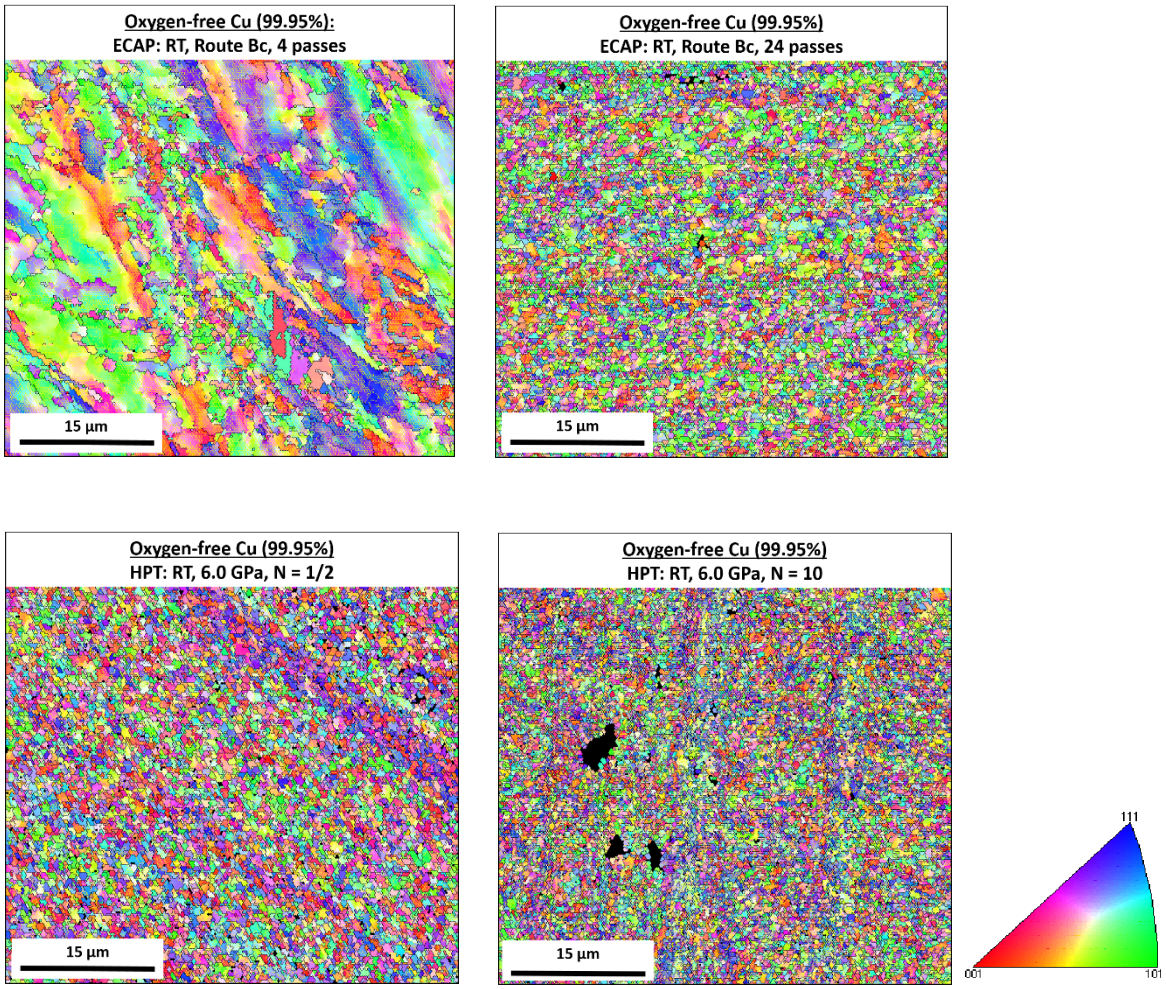

Fig. 2 EBSD orientation images show the evolution of microstructure in oxygen-free copper specimens after ECAP processing through a) 4 passes, b) 24 passes and after HPT processing through c) 1/2 turn, d) 10 turns.

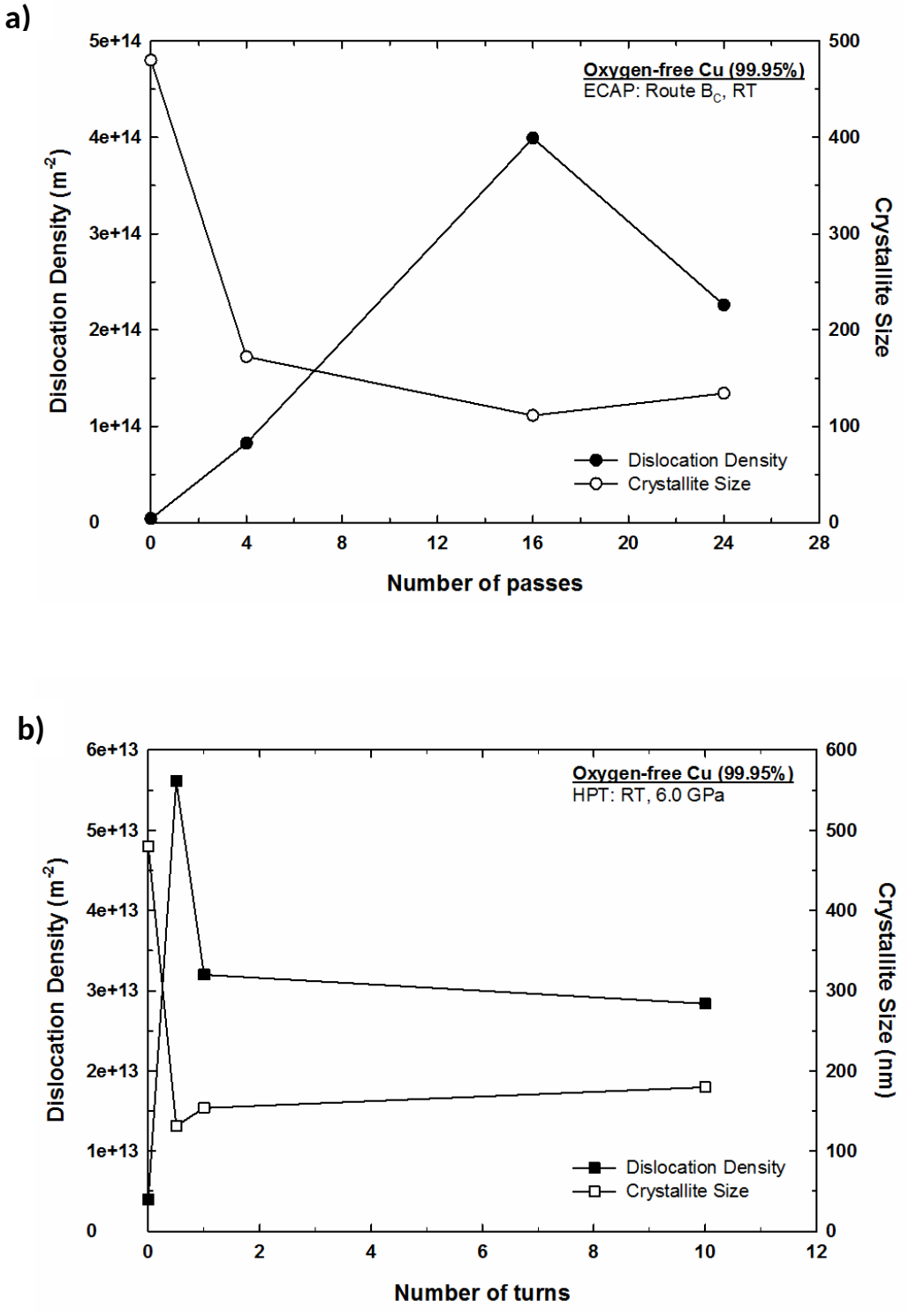

Fig. 3 Dislocation density and crystallite size as a function of the number of a) ECAP passes and b) HPT turns.

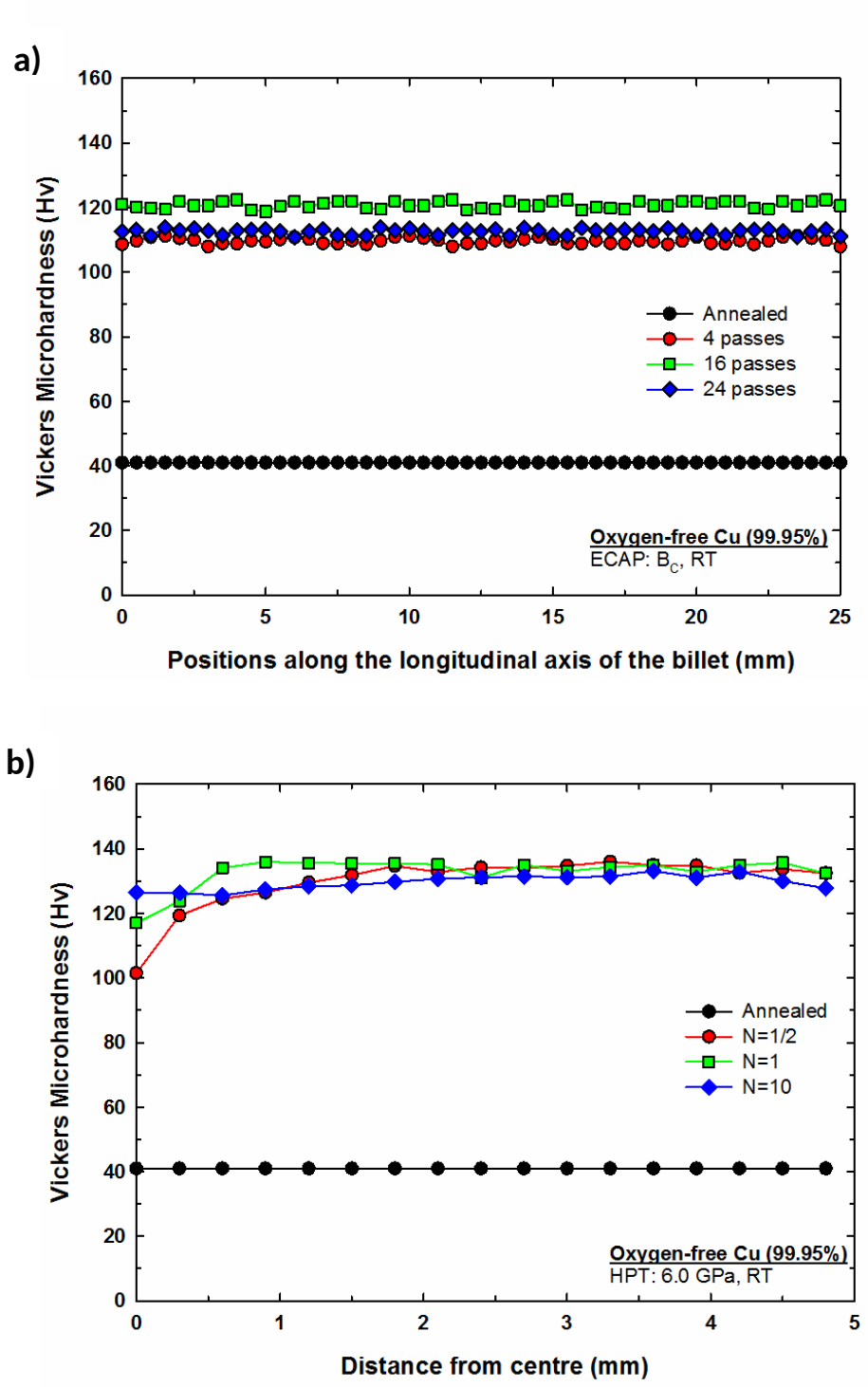

Fig. 4 Vickers microhardness measurements for oxygen-free Cu a) along the longitudinal axis of the ECAP billet and b) along the radius of the HPT discs.

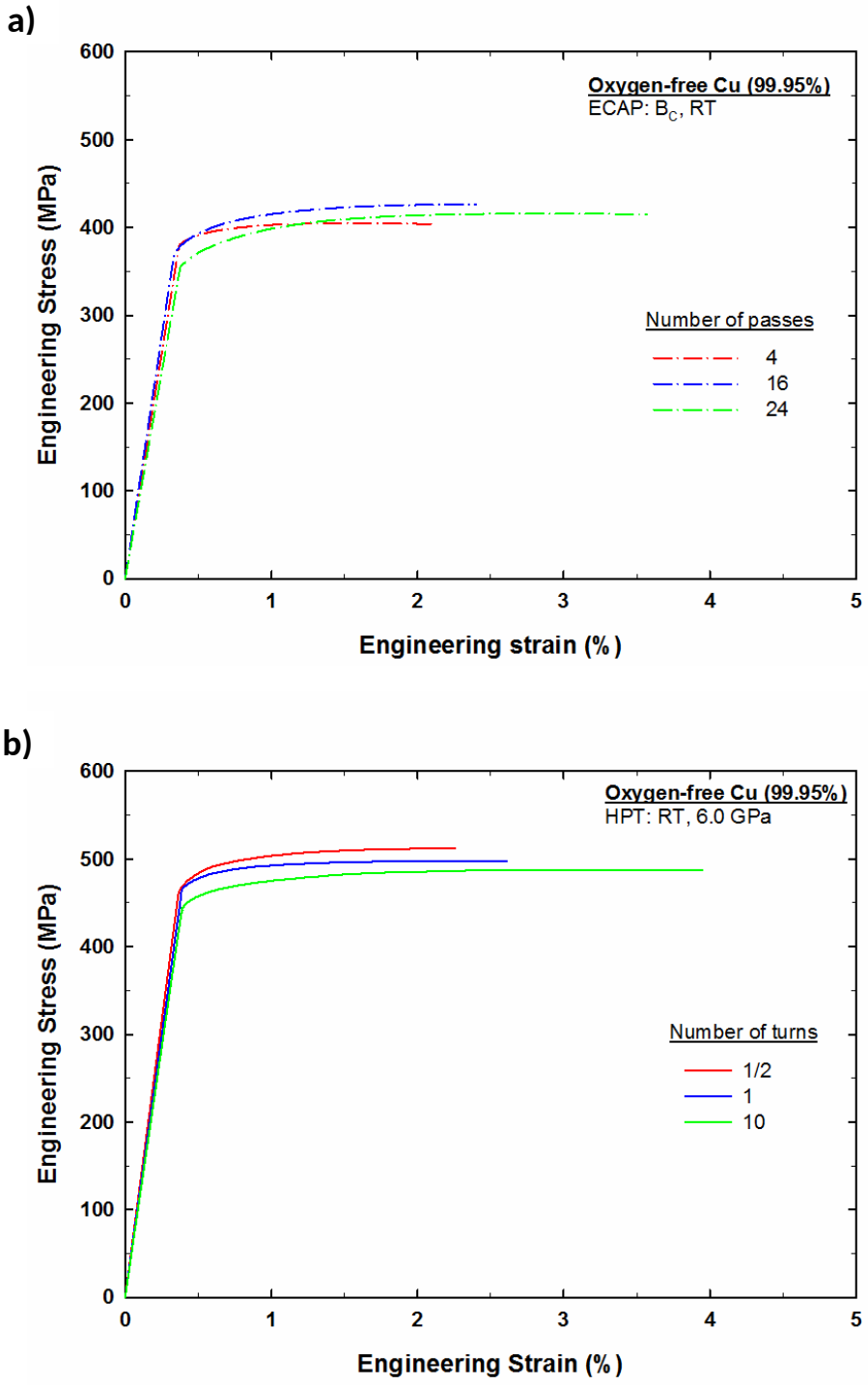

Fig. 5 Truncated true stress – true strain curves demonstrating the strain hardening behaviour for a) ECAP and b) HPT specimens.

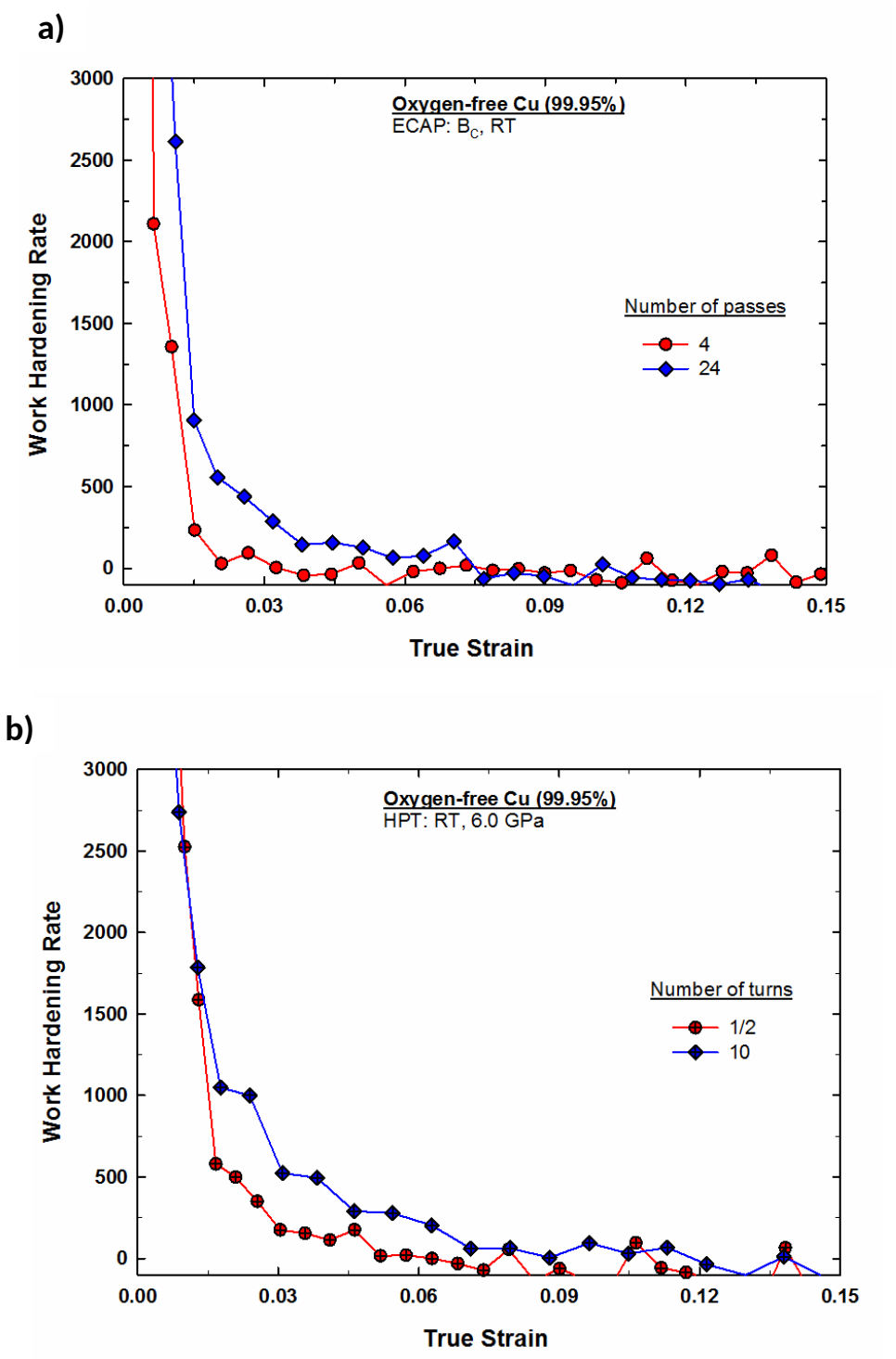

Fig. 6 Work hardening rate as a function of true stress for oxygen-free Cu deformed by a) ECAP and b) HPT.

Table 1. Values of yield stress (YS), ultimate tensile stress (UTS) and uniform elongation (UEL%) for Cu specimens subjected to HPT and ECAP.

Process Condition	**YS (MPa)**	**UTS (MPa)**	**UEL (%)**
4 passes	382	404	2.1
16 passes	376	426	2.4
24 passes	358	415	3.6
½ turn	474	512	2.0
1 turn	464	497	2.6
10 turns	444	487	4.0